A Bioinspired Nickel(bis-dithiolene) Complex as a Homogeneous Catalyst for Carbon Dioxide Electroreduction

Thibault Fogeron, Tanya K Todorova, Jean-Philippe Porcher, Maria Gomez-Mingot, Lise-Marie Chamoreau, Caroline Mellot-Draznieks, Yun Li, Marc Fontecave

A Bioinspired Nickel(bis-dithiolene) Complex as a Homogeneous Catalyst for Carbon Dioxide Electroreduction

Thibault Fogeron,[a] Tanya K. Todorova,[a] Jean-Philippe Porcher,[a] Maria Gomez-Mingot,[a] Lise-Marie Chamoreau,[b] Caroline Mellot-Draznieks,[a] Yun Li*[a] and Marc Fontecave*[a]

[a] Laboratoire de Chimie des Processus Biologiques, UMR 8229 CNRS, Collège de France, Université Paris 6, 11 Place Marcelin Berthelot, 75231 Paris Cedex 05, France.

[b] Sorbonne Universités, UPMC Université Paris 6, Institut Parisien de Chimie Moléculaire, UMR 8232 CNRS, 4 place Jussieu, 75252 Paris Cedex 5, France.

ABSTRACT

Inspired by the metal active sites of formate dehydrogenase and CO-dehydrogenase, a nickel complex containing a NiS_4 motif with two dithiolene ligands mimicking molybdopterin has been prepared and structurally characterized. During electroreduction, it converts into a good catalyst for the reduction of CO_2 into formate as the major product, together with minor amounts of carbon monoxide and hydrogen, with reasonable overpotential requirement, good faradaic yield and notable stability. Catalysis operates on a mercury electrode and dramatically less on a carbon electrode, as observed in the case of $[Ni(cyclam)]^{2+}$ complexes. DFT computations indicate the key role of a Ni(III)-hydride intermediate and provide insights into the different reaction pathways leading to HCOOH, CO and H_2. This study opens the route towards a new class of mononuclear sulfur-coordinated Ni catalysts for CO_2 reduction, unexplored yet.

KEYWORDS: dithiolene ligands, homogeneous catalysis, CO_2 reduction, Nickel, density functional calculations.

INTRODUCTION

Carbon dioxide 2-electron reduction into the energy-rich products, such as carbon monoxide (CO) and formic acid (HCOOH), offers the opportunity to develop synthetic organic reactions using CO_2 as a source of carbon, providing an alternative to fossil sources, as well as a way to store renewable energies into chemical energy durably. For such electrochemical processes, molecular catalysts have several substantial benefits.[1,2] First, their activity (reaction rates and overpotentials) can be finely tuned via simple modifications of the electronic properties of the organic ligands. Second, they are in general quite selective. In particular competition with proton reduction can also be controlled synthetically.[3] As a consequence, during the last 40 years a number of molecular complexes have been studied for their catalytic activity for CO_2 electroreduction into CO/HCOOH.[1,2] However, the best catalysts so far are based on expensive noble metals, such as rhenium, iridium, rhodium and ruthenium.[4,5] There are exceptions, notably the Fe-porphyrin systems developed by Savéant, Costentin and Robert,[6] but also some cobalt, iron and manganese complexes.[1,2,7]

Surprisingly there is a very limited contribution of Ni complexes so far, the prototype being $Ni(cyclam)^{2+}$, a catalyst with excellent activity in aqueous solutions and highly selective for CO production, developed in the 80's by Sauvage and collaborators and revisited by several groups recently.[8-14] Examples of Ni-based catalysts are: (i) Ni-polypyridine systems, such as $[Ni(bipy)_3]^{2+}$, $[Ni(phen)_3]^{2+}$, and $Ni(terpy)_2]^{2+}$ (bipy, phen, terpy = bipyridine, phenanthroline, and terpyridine respectively) which catalyze the selective conversion of CO_2 into CO, albeit with large overpotential requirements and low Faradaic yields;[1,15] (ii) Ni complexes supported by N-heterocyclic carbene-amine ligands and displaying high selectivity and activity for the electrocatalytic and photocatalytic conversion of CO_2 to CO;[16] (iii) very recently, a Ni complex bearing a S_2N_2–type tetradentate ligand which was found to selectively catalyze CO_2 reduction to CO in a visible-light-driven photocatalytic system.[17]

In the quest for new Ni-based molecular catalysts for CO_2 electro-reduction, we were intrigued by the possibility to explore Ni complexes supported by bioinspired ligands, with a specific interest for those ligands providing a sulfur-rich environment to the metal ion. Several lines of evidence point to the importance of sulfur ligation in active sites of metalloenzymes catalyzing CO_2 reduction. First, in one class of CO-dehydrogenases, a redox active Ni center is ligated by three S atoms, two provided

by sulfide from an iron-sulfur cluster and one by a cysteine residue, and catalyzes the reduction of CO_2 to CO.[18] In a second class of Mo/Cu CO-dehydrogenase[19] as well as in formate dehydrogenase, which catalyzes the reduction of CO_2 into formate, the metal center is composed of molybdenum (or tungsten) ions chelated by one or two dithiolene ligands provided by molybdopterin.[20,21] The objective of this work is to investigate bis-dithiolene complexes of nickel as catalysts for CO_2 electroreduction. A few Ni(bis-dithiolene) complexes, using benzene-1,2-dithiolate,[22] diaryl-dithiolene[23] or 5,6-dicyanopyrazine-2,3-dithiolate[24] as ligands, have been recently shown to catalyze proton electroreduction into H_2. However, to the best of our knowledge, there is no report of such complexes as catalysts for CO_2 reduction.

Here, we report the first Ni(bis-dithiolene) complex, and at the same time the first Ni complex having a NiS_4 coordination, that can perform catalytic reduction of CO_2. It contains a quinoxaline-pyran-fused dithiolene ligand, **qpdt^{2-}** (Figure 1) that mimics the natural molybdopterin cofactor (**MPT**, Figure 1) present in the active site of formate dehydrogenase and CO-dehydrogenase. This bioinspired ligand has been previously used to obtain the $(Bu_4N)_2[Mo^{IV}O(qpdt)_2]$ and $(Et_4N)_2[Co^{III}(qpdt)_2]_2$ complexes, which proved to be good catalysts for proton reduction.[25,26]

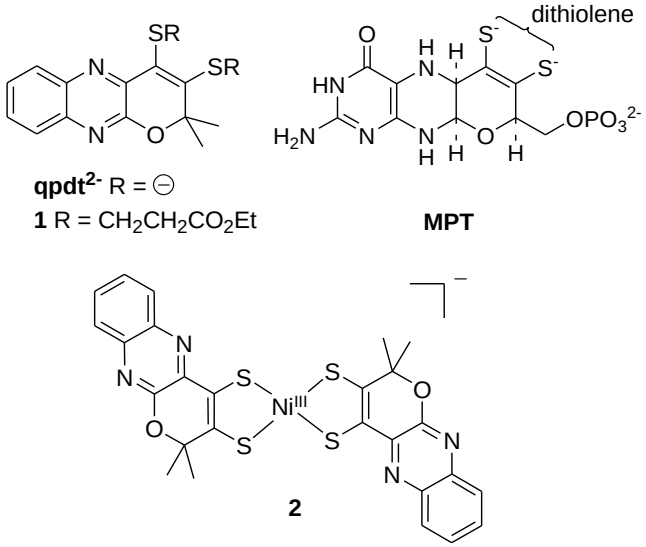

Figure 1. Structures of ligand $qpdt^{2-}$ in its protected form **1**, molybdopterin (MPT) and $[Ni^{III}(qpdt)_2]^-$ (**2**).

The synthesis, structural characterization and electrochemical properties of the nickel complex $[Ni^{III}(qpdt)_2]^-$ are thus described. This complex allows catalytic electroreduction of CO_2 into formate as the major product together with small amounts of CO and H_2, with remarkable stability, good faradaic yield and reasonable

overpotential requirements. Similar to $[Ni(cyclam)]^{2+}$ complex, catalysis is greatly promoted by interactions between the complex and the surface of the Hg electrode.[12] Density functional theory (DFT) computations were performed to explore possible reaction pathways for the CO_2 reduction catalyzed by the $[Ni(qpdt)_2]^-$ catalyst and to explain how the mixture of products can be formed.

RESULTS

Synthesis and characterization of the $[Ni^{III}(qpdt)_2]^-$ complex

Starting from the previously described protected dithiolene derivative **1**,[25,27] complex **2** was synthesized (see Figure 1 for the structures of **1** and **2**): compound **1** was treated with *t*BuOK under anaerobic conditions to generate the dithiolene ligand $qpdt^{2-}$ *in situ*; then reaction with $Ni(ClO_4)_2.2H_2O$ followed by cation exchange with Ph_4PCl afforded the square-planar complex $(Ph_4P)[Ni^{III}(qpdt)_2]$ (**2a**) in 52% yield. The redox active Ph_4P^+ counter-cation is reducible at −1.8 V *vs.* Ag/AgCl (Figure S1) which is within the range of potentials for catalysis. Thus all CO_2 electroreduction experiments were conducted with the same complex having Bu_4N^+ as the counter-cation, namely $(Bu_4N)[Ni^{III}(qpdt)_2]$ (**2b**). Both **2a** and **2b** are air-stable and can be purified by chromatography over silica gel. However only **2a** could be structurally characterized.

Single crystals suitable for X-ray diffraction were isolated for **2a** by layering a CH_2Cl_2 solution of the complex with pentane. A summary of the crystal data collection and refinement parameters are listed in Table S1. Selected interatomic bond lengths and angles are given in Table S2. An ORTEP-like diagram of the anionic part of **2a** is shown in Figure 2. Complex **2a** crystallizes in the monoclinc system and the unit cell includes four mononuclear complexes and four Ph_4P^+ ions. The Ni cation is tetra-coordinated in a S_4 environment with a square planar geometry. The four sulfur atoms belong to two symmetric *trans*-oriented $qpdt^{2-}$ ligands. The Ni–S bond lengths (2.1445(3) and 2.1536(3) Å) are similar to those reported previously for Ni(bis-dithiolene) complexes.[23]

Complex **2a** is soluble in common solvents (CH_2Cl_2, THF, CH_3CN, DMF). Its UV-visible spectrum in CH_3CN (Figure S2) shows five absorption maxima at 975, 627,

410, 392 and 314 nm with molar extinction coefficients ε = 18240, 6400, 37040, 34400 and 30400 $M^{-1}.cm^{-1}$ respectively. **2a** is paramagnetic and thus, no NMR spectrum could be recorded. The negative-ion electrospray mass spectrum in acetonitrile solution exhibits one peak at m/z = 605.95 ($[Ni(qpdt)_2]^-$), which is consistent with the structure (Figure S3).

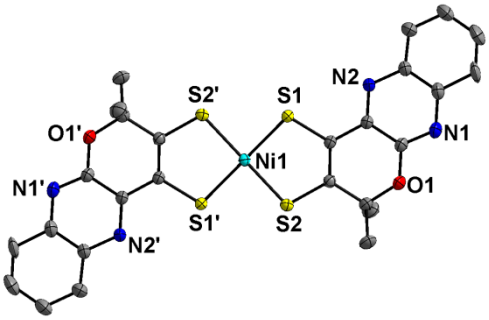

Figure 2. X-ray structure of $[Ni^{III}(qpdt)_2]^-$ (within **2a**) at 50 % probability. Hydrogen atoms are omitted for clarity.

The X-band EPR spectrum of **2a** in dichloromethane at 6 K (Figure S4) exhibits a sharp EPR signal (g = 2.002), which is similar to the previously reported spectrum recorded for $(PPh_4)[Ni^{III}(S_2C_2R_2)_2]$ complex (R = CO_2Me),[28] suggesting a ligand–centered radical. It is thus more appropriate to describe **2a** as $(PPh_4)[Ni^{II}(qpdt^{2-})(qpdt^{\bullet-})]$ rather than $(PPh_4)[Ni^{III}(qpdt^{2-})_2]$.

Figure 3 shows the cyclic voltammograms (CVs) of **2b** in dry acetonitrile on a glassy carbon electrode (GCE) (Figure 3A) and a mercury/gold amalgam electrode (Figure 3B). Under a N_2 atmosphere, **2b** displays a reversible wave at – 0.39 V corresponding to the $[Ni(qpdt)_2]^-$/ $[Ni(qpdt)_2]^{2-}$ couple and an irreversible wave at – 2.08 V on a GCE (Figure 3A). The peak current at – 0.39 V displays a linear relation to the square root of the scan rate, proving a diffusion-controlled electrochemical process typical for molecular complexes (Figure S5). The CV obtained on the Hg/Au electrode is essentially identical to the previous one, with the exception of the presence of a tiny additional feature at – 0.9 V (Figure 3B). This signal is likely reflecting the adsorption of the complex on the Hg electrode as reported for the case of $[Ni(cyclam)]^{2+}$ complexes.[8,10,12]

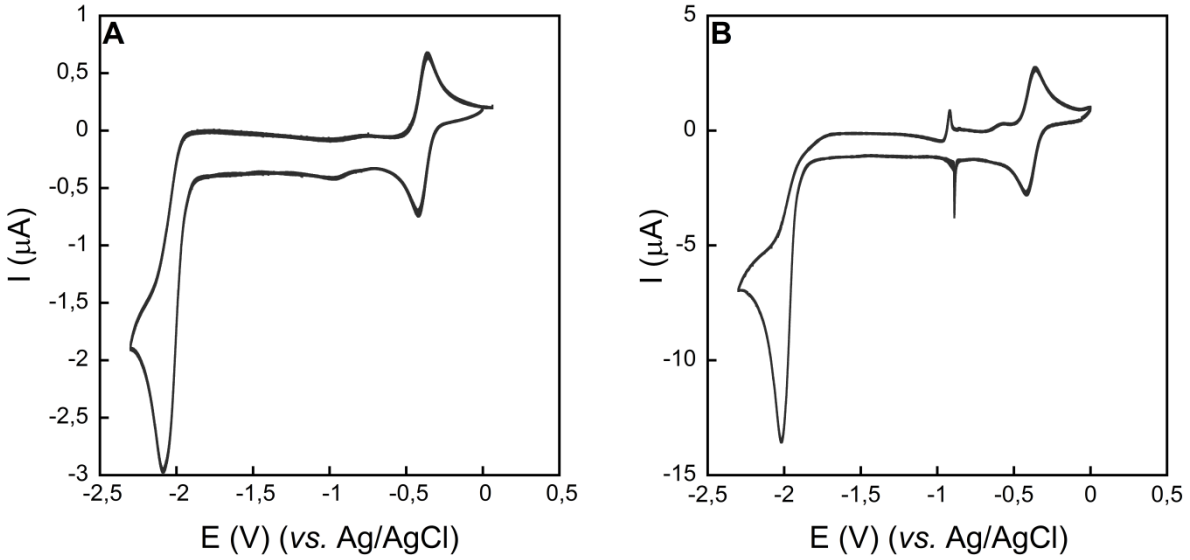

Figure 3. Cyclic voltammogram of 0.5 mM complex **2b,** 0.1 M tetrabutylammonium perchlorate (TBAP) under Ar in dry acetonitrile (CH_3CN) (**A**) on a GCE (glassy carbon electrode), (**B**) on a Hg/Au amalgam electrode. Scan rate: 50 $mV.s^{-1}$; third scan is shown.

Catalytic CO_2 electroreduction studies

The CV of a solution of complex **2b** did not change upon saturation with CO_2, in the absence of a source of protons (Figure 4). Addition of 2 M trifluoroethanol (TFEH) led to a large catalytic wave, however observed only on the Hg/Au electrode (Figure 4). Indeed a large difference between the glassy carbon electrode (GCE) and the Hg/Au electrodes was observed (Figure S6). This behavior is reminiscent of that observed in the case of the $[Ni(cyclam)]^{2+}$ complex. In that case, it was proposed that favorable interactions between the complex and the Hg surface of the electrode resulted in a dramatic enhancement of the catalytic efficiency of the complex.[8,10,12] Therefore, herein we present only data obtained with the Hg/Au electrode.

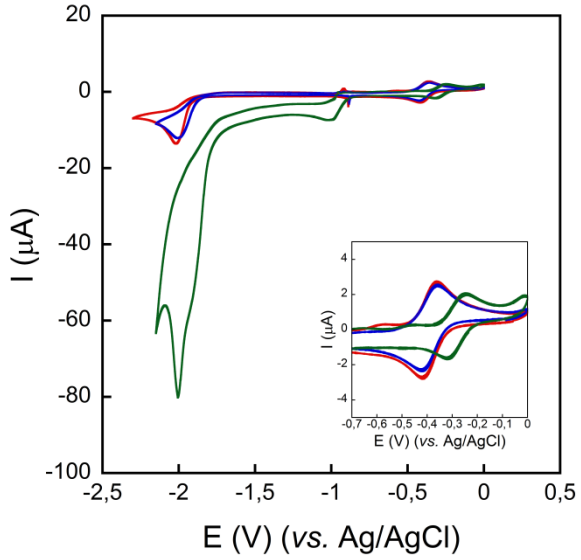

Figure 4. Cyclic voltammograms of 0.5 mM of complex **2b** under an Ar atmosphere (red line) and under a CO_2 atmosphere, without (blue line) and with 2 M TFEH (green line) in CH_3CN with 0.1 M TBAP. Scan rate 50 $mV.s^{-1}$; Hg/Au amalgam electrode; third scan is shown. Inset: Zoom on the $[Ni(qpdt)_2]^{-}/[Ni(qpdt)_2]^{2-}$ wave.

Several features of the CV of **2b** in CH_3CN in the presence of CO_2 and 2 M TFEH on a Hg/Au electrode (Figure 4) should be considered. First, the $[Ni(qpdt)_2]^{-}/[Ni(qpdt)_2]^{2-}$ wave was shifted 120 mV anodically indicating that reduction is eased by protonation. Second, the onset potential of the catalytic wave is at about – 1.7 V, with a half-wave potential at – 1.80 V and a peak at – 2 V, thus resulting in an overpotential of approximately 340 mV. Even though several products were formed, but with formate being the major product of the reaction (see below), the overpotential was determined by comparing the experimental onset potential to the standard potential of the CO_2/HCOOH couple in CH_3CN in the presence of TFEH as a proton source (see SI for calculation details). Third, a new irreversible wave was observed at – 1 V. This feature is reminiscent of that observed in the CV of the $[CpCo^{III}(qpdt)]$ complex (**3**), in an organic solvent and in the presence of a source of protons.[29] In that case we have clearly demonstrated, via electrolysis at this potential, isolation and characterization of the reaction product, that this redox feature corresponds to an O1-C2 bond cleavage of the pyran ring upon a 4-electron reduction of the dithiolene ligand (Scheme 1).

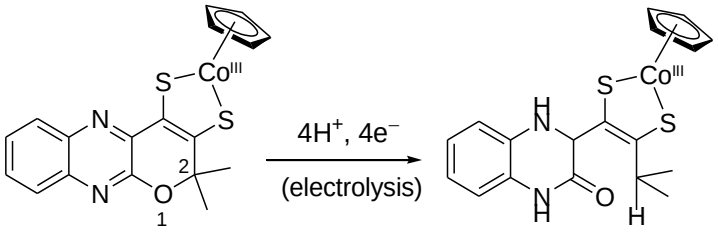

3 [Co^{III}Cp(qpdt)]

Scheme 1. O1-C2 bond cleavage of the pyran ring upon a 4-electron reduction of [CpCo^{III}(qpdt)]. (ref. 26)

We have applied the same strategy for the $[Ni^{III}(qpdt)_2]^-$ complex, but we failed to isolate a stable product after electrolysis. However, at a low scan rate (1 mV.s^{-1}), analysis of the irreversible wave at – 1 V allowed us to estimate that it fitted with an 8-electron process, most likely corresponding to the 4-electron reduction of each $qpdt^{2-}$ ligand of complex **2b** as in the case of the Co complex (Figure S7). Hence, the CV data indicate that complex **2b** is in fact a catalyst precursor and that complex **4**, derived from reduced **2b**, $[Ni^{II}(qpdt)_2]^{2-}$, through a full reduction of the ligand at the applied catalytic redox potential and subsequent pyran ring opening, is instead the real catalyst (Scheme 2). Accordingly, the CV of the solution after electrolysis showed that the initial complex **2b** was no longer present and that another complex was formed. It is characterized by two quasi-reversible redox waves, at + 0.04 V and at – 0.8 V (Figure S8). We assigned these features to the Ni(IV)/Ni(III) and Ni(III)/Ni/(II) couples for complex **4.** The cathodic shift of ~ 550 mV with respect to **2b** is consistent with a more reduced ligand system.

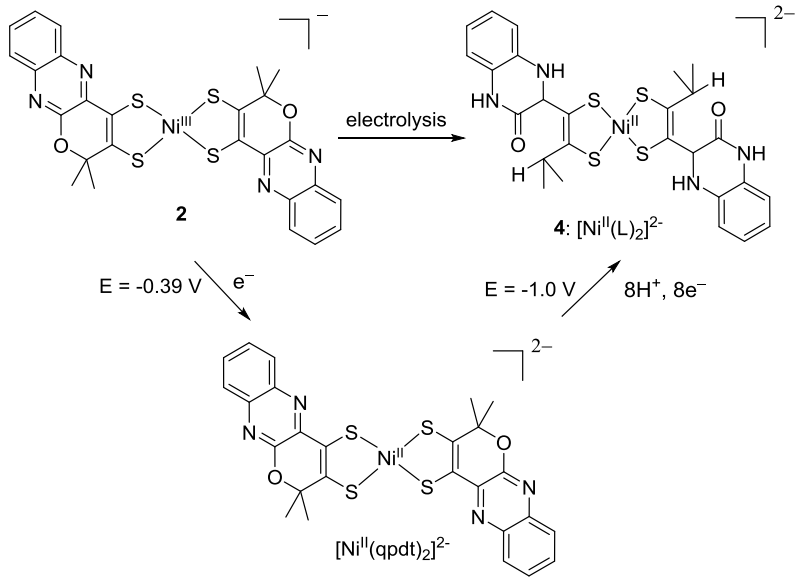

Scheme 2. Conversion of $[Ni(qpdt)_2]^-$ into complex **4** during electrochemical reduction.

Finally, in order to verify that no complex was permanently adsorbed on the Hg surface, a rinse test experiment was carried out. After 50 cycles in a solution containing 0.5 mM complex and 2 M TFEH under CO_2 atmosphere, the electrode was carefully rinsed and then assayed again in a freshly prepared solution without catalyst. As shown in Figure S9, no catalytic wave could be observed anymore. In order to evaluate the impact of the ligand on the observed activity, complex $(Bu_4N)[Ni^{III}(S_2C_2R_2)_2]$ (**5**, R = CO_2Me), synthesized according to a previously published procedure,[28] was studied and compared to complex **2b**. As it can be seen in Figure S10, no catalytic activity was found.

The reaction products were identified and monitored during electrolysis performed at – 1.9 V on a 1 cm diameter mercury pool working electrode (Figure S11). After 15 min, the current reached a value of about – 1.6 mA and remained stable for 4 hours. Formic acid was shown to be the main product (9 TONs after 4 hours and 60 % faradaic yield (FY)). Minor amounts of CO (3 TONs, 19%) and H_2 (1.5 TONs, 9%) were also formed, giving a total FY close to 90%. Faradaic yields were calculated taking into account that 8 e^- are required up for the reduction of the ligands and that 2 e^- are mandatory to activate the metal center and initiate the catalysis. As observed in Figure S11, in the absence of catalyst the current was much less intense (0.5 mA) and the production of formate and carbon monoxide was negligible (Table S3). According to literature procedures, the electrolysis data were used to estimate a TOF value of 89 s^{-1} for the electrocatalytic reduction of CO_2 at - 1.9 V (see SI for details of the calculation).[30,31] A longer electrolysis (23 h) reveals the remarkable stability of the catalyst (Figure S12). The current was stabilized at 1 mA during the first 15 hours, after which it started to decrease. Product formation was sustained during the 23 hours of reaction leading to 38 TONs of formic acid (51% FY) along with 7.5 TONs of CO (10 %) and 6.5 TONs of H_2 (8.5%). Finally, the selectivity of the reaction was unchanged when electrolysis was performed at different potentials in the range of – 1.75 V to – 2.1 V.

Several control electrolysis experiments were carried out (Table S4). First, no CO_2 reduction catalytic activity could be observed using $Ni(ClO_4)_2$ instead of complex **2b**, thus excluding the presence of active Ni particles derived from degradation of the

complex during the reactions catalyzed by **2b**. Second, a rinse test showed that the complex was not irreversibly attached to the surface of the Hg pool. Third, when a GC electrode (1 cm diameter) was used as a working electrode, the current was not stable (Figure S13) and only very small amounts of products were detected (Table S4). Fourth, in agreement with the CV experiments (Figure S14), weaker acids such as MeOH or water failed to stimulate catalysis. Electrolysis at − 1.9 V for 4 hours in the presence of 2.7 M of H_2O or 2 M of MeOH led to much lower formation of products, poor selectivity for the reduction of CO_2 and low faradaic yields (Table S5). Large currents were observed in the presence of a stronger acid such as phenol (Figure S15), but a 4-hour electrolysis experiment at − 1.9 V (Table S5) revealed that they were essentially originating from proton reduction into H_2. Finally, a larger concentration of TFEH (3 M) resulted in increased production of H_2, while a 0.5 M TFEH solution was not acidic enough.

Computational investigation of the CO_2 reduction mechanism.

*Electronic structure of **2** and **4***. The $[Ni(qpdt)_2]^-$ complex **2** was fully optimized starting from its experimental X-ray crystal structure. Table S6 summarizes selected bond lengths and angles, showing that the two geometries are in excellent agreement (bond lengths are within 0.02 Å of the values in the crystal structure and the bond angles are within 1°). The ground state of **2** is a doublet, which is in agreement with our EPR analysis (Figure S4). The unpaired electron is localized on the dithiolene moiety of the $qpdt^{2-}$ ligands and has mainly S_{3pz} and C_{2pz} character as indicated by the SOMO orbital in Figure S16a. Due to the redox non-innocent nature of the dithiolene ligands, the structure can be represented by two resonance structures $[Ni^{III}(qpdt^{2-})_2]^- \leftrightarrow [Ni^{II}(qpdt^{2-})(qpdt^{\bullet-})]^-$, with the radical anion character being the dominant form. Direct one-electron reduction to $[Ni^{II}(qpdt)_2]^{2-}$ is computed to occur at a potential of E^0 = − 0.69 V *vs*. Ag/AgCl electrode (experimental E^0 = − 0.39 V). The Ni ion remains as a Ni^{II} center because the extra electron goes to a dithiolene ligand orbital (Figure S16b). The $[Ni(qpdt)_2]^{2-}$ system has a closed-shell singlet ground state (S = 0), while the triplet state is 5.7 kcal mol^{-1} higher in energy. The square-planar structure of complex **2** is preserved in its one-electron reduced form accompanied by elongation of the Ni–S bond lengths by ~0.03 Å (Table S6).

Since the real catalyst is likely complex **4**, all further DFT computations have been performed with **4**, referred here as $Ni^{II}(L)_2]^{2-}$, L being the open ligand (Scheme 2). **4** has a singlet ground state, which is 4.5 kcal mol^{-1} more favored than the triplet state. Moreover, inspection of the bond lengths and angles (Table S6) indicates that the geometry of its Ni dithiolene moiety remains very similar to that of the one-electron reduced complex **2**, $[Ni^{II}(qpdt)_2]^{2-}$. Electron reduction of **4** occurs at a computed reduction potential $E^0 = -2.31$ V *vs*. Ag/AgCl and leads to the formation of a $Ni^{I}(L)_2]^{3-}$ species bearing a Ni^{I} center (see Figure S17), along with a significant elongation of the Ni–S bonds by ~ 0.15 Å (Table S6).

CO_2 adducts. While only side-on η^2-CO_2 nickel structures have been reported to date,[32-35] most theoretical studies on low-coordinate Ni centers revealed that both η^1-CO_2 and η^2-CO_2 are energetically favored coordination modes.[36-38] In this work, we have located two different binding modes of CO_2 to the Ni center, namely the η^1-CO_2 and η^1-OCO. Comparison of their geometries and binding parameters are given in Table S7. Our calculations strongly favor the η^1-CO_2 binding mode in $[Ni(\eta^1\text{-}CO_2)(L)_2]^{3-}$, while the η^1-OCO adduct, $[Ni(\eta^1\text{-}OCO)(L)_2]^{3-}$, is 19 kcal mol^{-1} higher in energy. We could not locate a stable η^2-CO_2 complex, as during the geometry optimization the initial $[Ni(\eta^2\text{-}CO_2)(L)_2]^{3-}$ structure rearranges to the stable $[Ni(\eta^1\text{-}CO_2)(L)_2]^{3-}$ one. It is important to note that no CO_2 adduct can be formed starting from complex **4**. Instead, a one-electron reduction step has to take place in order to create the active intermediate $[Ni^{I}(L)_2]^{3-}$, which can further undergo two possible reaction pathways, as depicted in Figure 5 (*vide infra*).

The $[Ni(\eta^1\text{-}CO_2)(L)_2]^{3-}$ CO_2 adduct is characterized by a bending of the CO_2 molecule when coordinated to the Ni center, with a O–C–O angle of ~ 135°. Additionally, the two C–O bonds are considerably elongated by ~0.07 Å and resemble those for $CO_2^{\bullet-}$ (Table S7). Molecular orbital (MOs) analysis shows that the electronic structure of $[Ni(\eta^1\text{-}CO_2)(L)_2]^{3-}$ is best described as Ni^{II}–$CO_2^{\bullet-}$, which implies that the electron reduction of CO_2 is nearly completed (Figure S18).

DFT mechanistic pathways. The CO_2 electrochemical reduction results in formation of formate, CO, and H_2, with formate being the main product. Figure 5 shows the DFT proposed mechanistic pathways towards the formation of the observed

products. The η^1-OCO complex may directly transform into a nickel formate species $[Ni(OCOH)(L)_2]^{2-}$ via uptake of a proton as suggested for $Ni(cyclam)^+$.[13] However, as mentioned above, this $[Ni(\eta^1\text{-}OCO)(L)_2]^{3-}$ adduct is computed to be strongly disfavored and cannot be regarded on the operating route for the production of formate. Therefore, our calculations invoke a Ni-hydride intermediate $[Ni^{III}(H)(L)_2]^{2-}$ as a catalytically relevant species. It is formed upon protonation of the reduced complex **4** and has a transition state barrier of 14.0 kcal mol^{-1} (computed with the TFEH homoconjugate complex as an explicit proton source). Its frontier molecular orbitals are shown in Figure S19. Exergonic by 7.3 kcal mol^{-1}, the nickel hydride formation results in a $Ni^{III}(H)$ center in a tetragonal coordination with respect to the two dithiolene ligands. Protonation of the different S atoms is + 1.0 and + 3.6 kcal mol^{-1} higher in energy. The $[Ni^{III}(H)(L)_2]^{2-}$ species then reacts with CO_2 and a transition state was located with a free energy of activation of only 7.1 kcal mol^{-1}. Direct subtraction of the proton through an internal hydride transfer in the $[Ni\cdots HCO_2^-]$ complex is followed by a release of $HCOO^-$ (ΔG = – 32.9 kcal mol^{-1}) and regeneration of the catalyst **4** upon one-electron reduction step at E^0 = – 0.51 V (red pathway in Figure 5).

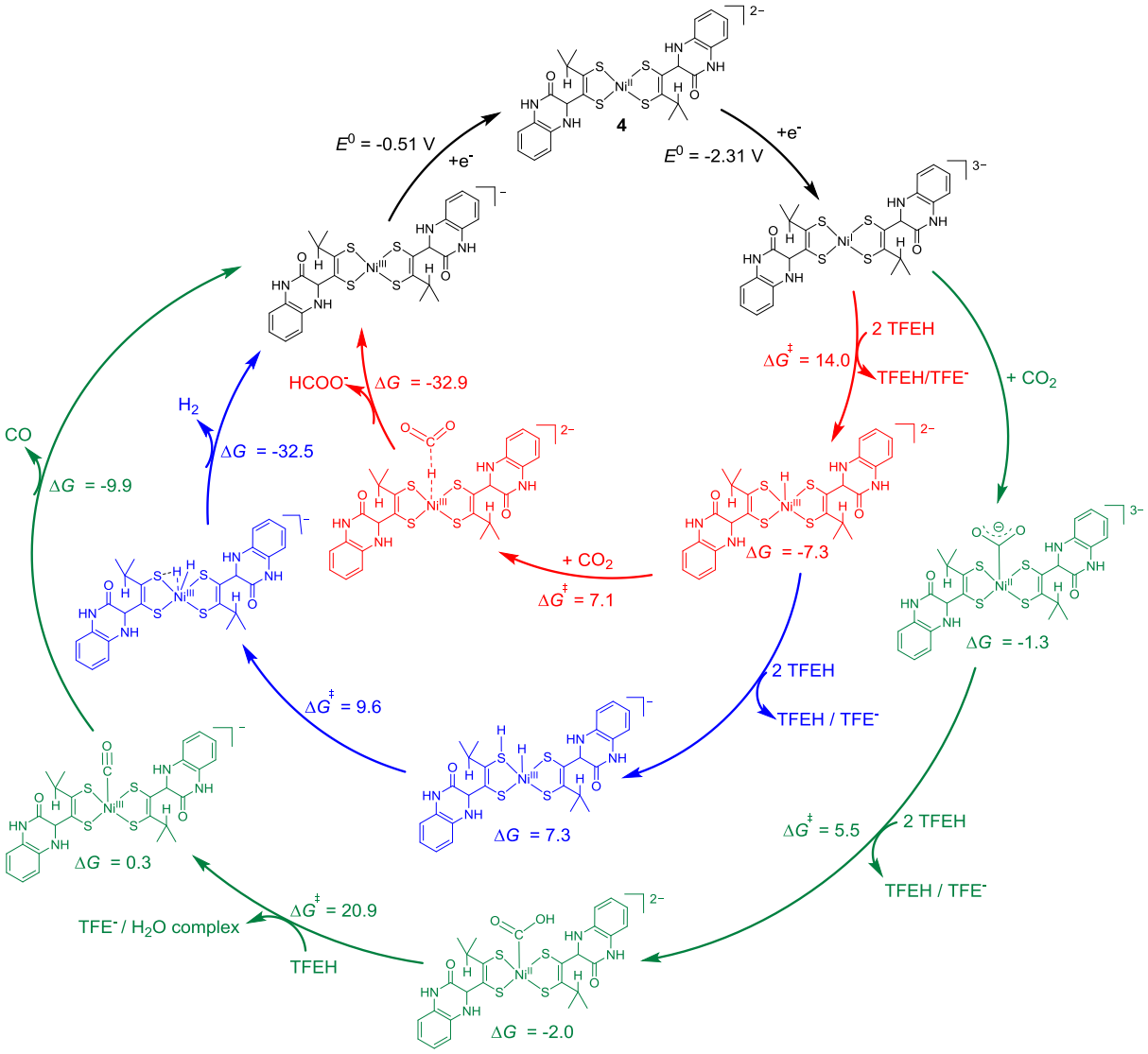

Figure 5. Proposed reaction mechanisms of CO_2 reduction by complex **4** to formate (red), H_2 (blue), and CO (green). The relative Gibbs free energies (ΔG, kcal mol^{-1}) and transition state barriers ($\Delta G^{\#}$, kcal mol^{-1}) are reported relative to the preceding intermediate. Standard one-electron reduction potentials (E^0, V) are given *vs.* Ag/AgCl electrode.

The Ni-hydride $[Ni^{III}(H)(L)_2]^{2-}$ intermediate has a key role in the formation of H_2. It can accept a second proton from the acid source to form $[Ni^{III}(H)(SH)(L)_2]^{-}$ species (ΔG = + 7.3 kcal mol^{-1}). The protonation occurs on a sulfur atom from the dithiolene ligand with an S–H bond *syn* to the Ni–H bond. This species is well set to release hydrogen with a computed transition state barrier of 9.6 kcal mol^{-1} (blue pathway in Figure 5).

Finally, the small amount of CO observed during the electrolysis can be explained by the reaction pathway (green pathway in Figure 5) proceeding through the η^1-CO_2 species (ΔG = – 1.3 kcal mol^{-1}). First, a protonation to the carboxylate intermediate $[Ni(C(O)OH)(L)_2]^{2-}$ takes place (ΔG = – 2.0 kcal mol^{-1}) and a transition state was

located with a free energy of activation of 5.5 kcal mol^{-1} (frontier MOs are shown in Figure S20). Subsequently, in the presence of another proton the carboxylate undergoes a heterolytic C–O bond cleavage to generate $[Ni(CO)(L)_2]^-$. This is the rate-limiting step, since the computed TS barrier amounts to 20.9 kcal mol^{-1}. The value is very similar to the corresponding barriers computed for CO_2 reduction by $Ni(cyclam)^+$ (20.9 kcal mol^{-1}),[13] $[Re(bpy)(CO)_3]$ (22.5 kcal mol^{-1}),[39] as well as $[Mn(bpy)(CO)_3]^-$ (22.2 kcal mol^{-1}).[40] The reaction is followed by a release of a CO molecule (ΔG = – 9.9 kcal mol^{-1}) and the recovery of complex **4** upon a one-electron reduction step.

DISCUSSION

Still only few classes of mononuclear complexes have been explored as catalysts for homogeneous CO_2 electroreduction and quite surprisingly, among non-noble metals, Ni has been much less studied than Co, Fe or Mn. One exception is the $[Ni(cyclam)]^{2+}$ complex and derivatives which proved excellent catalysts for the selective electroreduction of CO_2 into CO.[41] Complex **2**, $[Ni(qpdt)_2]^-$, reported here thus opens new perspectives in Ni-based CO_2 electroreduction catalysis as it shows that a Ni ion coordinated exclusively by S atoms (here NiS_4) displays very interesting catalytic performances. The only related precedent, reported during the course of this study, is a Ni complex bearing an S_2N_2-type tetradentate ligand which was shown to catalyze CO_2 reduction into CO in a photocatalytic system. Sulfur coordination to Ni is in fact one of the solutions found by Nature for interconverting CO_2 and CO, within [NiFe] CO-dehydrogenases (CODHs). Even though the NiFe cluster in CODH is much more complex than the synthetic compound **2**, exquisite biochemical and structural data have suggested the unique Ni center to play a major redox role during the enzyme reaction.[18] In a way, the demonstration here that catalysis for CO_2 reduction can be promoted just by a mononuclear S-coordinated Ni complex provides further support to the hypothesis that Ni is the only redox-active site in CODH and that the dangling Fe atom rather serves as a Lewis acid for polarizing a C–O bond for subsequent cleavage. As it is the first and unique example of this class of complexes, there are a lot of open questions regarding the influence of the ligands on the reactivity. Indeed, here a special ligand has been used, namely $qpdt^{2-}$, a molecule containing a bidentate dithiolene moiety and mimicking the molybdopterin ligand

present in formate dehydrogenases and [MoCu] CODH. The absence of activity found with complex **5,** bearing a simpler dithiolene ligand, proves that the ligand is playing a role in the catalysis and that it is not general to any Ni(bis-dithiolene) complex. Obviously, other S-based ligands need to be further investigated.

One implication of using this particular ligand resides in the fact that complex **2** is a catalyst precursor and complex **4** is the actual catalyst (Scheme 2). Indeed, we have shown that, when coordinated to a metal ion, $qpdt^{2-}$ undergoes a 4-electron reduction of its pyrazine ring at potential values more positive than that required for catalysis, followed by the opening of the pyran ring, leading to a new stable dithiolene ligand (L). As a consequence, DFT calculations aiming at getting insights into the CO_2 reduction mechanism have been carried out using complex **4**.

A final comment with respect to the true nature of the catalyst considers the importance of a mercury electrode for stimulating the catalytic activity of the Ni complex. Indeed, catalytic activity was dramatically enhanced on such an electrode as compared to a standard glassy carbon electrode. There are several precedents of Ni complexes, with a variety of ligands such as bipyridine,[42] glyoxime[43] and salen[44] adsorbing at Hg electrodes. But the most relevant example in the context of CO_2 reduction catalysis is $[Ni(cyclam)]^{2+}$ complex. A recent study[10] established that the dramatic increase in catalytic activity on mercury was due to favorable non-covalent interactions between the cyclam ligand and the surface of the mercury electrode, leading to the adsorption of the most active conformer and encouraging CO_2 binding. Additionally this facilitates CO desorption, the limiting step of the reaction, thus limiting CO poisoning. Even though this needs to be studied, we believe that similar scenarios are at work in the case of the Ni complex. Nevertheless, these observations suggest that specific non-covalent interactions between homogeneous catalysts and metallic surfaces, very little studied so far, play important roles, thus opening perspectives for improving catalytic performances.

The characteristics of the reaction catalyzed by complex **2** are the following: (i) catalysis starts at an onset potential corresponding to an overpotential of only 340 mV; (ii) electrolysis generates formate as the major product together with small amounts of CO and H_2 with good total faradaic yields close to 90%; (iii) the selectivity of the system can be optimized via an appropriate choice of the proton donor, with

TFEH providing the best balance for preventing too large production of H_2; (iv) the system is remarkably stable since sustained reduction of CO_2 was achieved during an electrolysis experiment of 23 h (Figure S11). At first sight, it seems that the system suffers from low selectivity.

Formation of formic acid as the major product is to be noted. While several Rh-, Ru- and Ir-based complexes have been shown to catalyze the electroreduction of CO_2 to formic acid,[4,5] examples based on non-noble metals are rare. This has been reported mainly in the case of Fe complexes[45-47] and a series of CpCo-diphosphine complexes.[48] Ni and Mn complexes are known to produce exclusively CO except under very particular conditions which promote formate production.[49,50] In the specific case of the $[Ni(cyclam)]^{2+}$ complex, it has been shown that even after reduction, the complex is not basic enough to react with protons and thus formation of a hydride Ni-H species, the generally proposed precursor for HCOOH and H_2 evolution, is excluded.[13] This thus explains the high selectivity of the catalyst for CO production: the nucleophilic reduced complex reacts exclusively with CO_2, giving an η^1-CO_2 adduct acting as a precursor of CO.[13] In DMF, formation of formic acid can therefore be explained only by formation and protonation of a η^1-OCO adduct, however strongly destabilized with regard to the former adduct.[13,50]

In contrast, in the case of complex **4**, DFT calculations reported here show that several pathways are possible, thus explaining the formation of the 3 products, i.e., formic acid, CO and H_2 (Figure 5). The reduced active $[Ni^{I}(L)_2]^{3-}$ intermediate can not only react directly with CO_2, opening the way to CO, as in the case of the $[Ni(cyclam)]^{2+}$ complex, but also to a Ni-hydride intermediate, which is responsible for the formation of formic acid and H_2. This is likely due to the stronger electron-donating properties of the dithiolene ligand in complex **4**, which allow the formation of a Ni-hydride intermediate, reactive enough to generate both formate and H_2 by reaction with CO_2 and H^+, respectively.

CONCLUSIONS

This study demonstrates for the first time that a molecular Ni(bis-dithiolene) complex has the potential to function as a rather efficient and stable catalyst for the electroreduction of CO_2. While it indeed opens the way to a new class of CO_2 reduction catalysts, investigation of a broader range of Ni complexes, with NiS_x

coordination, is needed to better understand structure-activity relationships and to optimize such systems.

AUTHOR INFORMATION

Corresponding Author

*E-mail: yun.xu-li@college-de-france.fr;

*E-mail: marc.fontecave@college-de-france.fr

ORCID

Yun LI : 0000-0003-4805-7156.

Marc Fontecave : 0000-0002-8016-4747.

Maria Gomez-Mingot : 0000-0002-1557-2648.

Notes

The authors declare no completing financial interest.

ASSOCIATED CONTENT

Supporting Information

The Supporting Information is available free of charge on the ACS Publications website at http://pubs.acs.org:

Electrochemical characterizations of complexes **2**, along with catalytic studies. Frontier molecular orbitals of **2** and **4**, the η^1-CO_2 adduct $[Ni(\eta^1\text{-}CO_2)(L)_2]^{3-}$, $[Ni(C(O)OH)(L)_2]^{2-}$ and the Ni-hydride $[Ni^{III}(H)(L)_2]^{2-}$, geometrical parameters for **2**, **4** and their reduced complexes, as well as geometrical and binding parameters for the located CO_2 adducts, xyz coordinates of all intermediates.

ACKNOWLEDGEMENTS

This work was supported by the French National Research Agency (CarBioRed ANR-12-BS07-0024-03, PhotoCarb ANR-16-CE05-0025-01), the Fondation de l'Orangerie

for individual Philanthropy, the French State Program ‘Investissements d’Avenir’ (Grants “LABEX DYNAMO”, ANR-11-LABX-0011). We are grateful to E. Galardon (University of Paris Descartes) and S. Blanchard (University of Pierre Marie Curie) for EPR analysis. We thank L. Dubost (Museum National d’Histoire Naturelle) for technical support and P. Simon for various CO_2 reduction products detection methods. The calculations were performed using the iDataPlex cluster of the UPMC DSI computing center and the HPC resources of GENCI (TGCC) through Grant 2017-810082.

EXPERIMENTAL SECTION

General Considerations

All reagents and solvents were used as received unless otherwise specified. Aqueous solutions were prepared with doubly deionized water with resistivity not less than 18.2 MΩ cm−1. Anhydrous acetonitrile (CH_3CN), tetra-*n*-butylammonium perchlorate were purchased from Sigma-Aldrich and used as received.

All ^1H NMR experiments were conducted on a Bruker 300 MHz instrument and the UV−vis spectra were recorded using a Cary 100 UV−vis spectrophotometer instrument (Agilent). Mass spectrometry analysis and electrospray Q-TOF (ES Q-TOF MS) were performed on a Q-star instrument (Applied Biosystem).

Synthesis of $(PPh_4)[Ni^{III}(qpdt)_2]$ (2a)

The experiment was carried out under Ar using Schlenk tubes and all solutions were degassed prior to use. *t*BuOK (189 mg, 1.67 mmol) was added to a solution of **1** (200 mg, 0.420 mmol) in anhydrous THF (4 mL). After 15 min at room temperature, a solution of $Ni(ClO_4)_2.6H_2O$ (76 mg, 0.210 mmol) in MeOH (1 mL) was added dropwise *via* a cannula needle to the dark red suspension. An immediate color change to black was observed. After 30 min, PPh_4Cl (157 mg, 0.42 mmol) was added and the dark green solution was kept at room temperature for 3 h. After evaporation of solvents, the dark green precipitate was dissolved in CH_3CN, filtered and evaporated to dryness. The crude product was purified by flash chromatography over silica gel (eluting with MeOH : CH_2Cl_2, 1:99) gave a dark green solid (103 mg, 52 %). UV-Vis (CH_3CN), λ_{max} nm (ε, M^{-1} cm^{-1}): 975 (18240), 627 (6400), 410 (37040), 392 (34400).

Negative-ion ESI-MS (CH_3CN): m/z = 605.98 ($[Ni(qpdt)_2]^-$) ; Anal. Calcd for $C_{50}H_{40}N_4NiO_2PS_4$ (946.8054): C 63.43, H 4.26, N 5.92, S 13.55; Found: C 63.60, H 4.08, N 5.82, S 13.67. Single crystals suitable for X-ray diffraction were obtained by layering pentane over a CH_2Cl_2 solution containing the crude complex at room temperature.

Synthesis of $(Bu_4N)[Ni^{III}(qpdt)_2]$ (2b)

The same procedure was applied except that *n*Bu_4NBr was used instead of PPh_4Cl. Anal. Calcd for $C_{42}H_{56}N_5NiO_2S_4$ (849.8764): C 59.36, H 6.64, N 8.24, S 15.09; Found: C 59.33, H 6.40, N 8.22, S 15.03.

Electrochemical experiments

All cyclic voltammetry (CVs) experiments were performed in a conventional three-electrode single-compartment cell with a SP 300 Bio-Logic potentiostat (Bio-Logic Science Instruments SAS). A saturated Ag/AgCl/KCl electrode (hereafter abbreviated as Ag/AgCl) was placed in the same compartment as the working electrode separated by a bridge with a Vycor frit and was used as the reference electrode. A platinum counter electrode was separated from the solution by a glass frit. Glassy carbon electrode (GCE from BASi) of 1 mm diameter or Hg/Au amalgam electrode were used as working electrodes. The Hg/Au amalgam electrode was prepared by dipping a 1.6 mm diameter disk Au electrode (BASi) into a pool of mercury. Electrodes were polished on wet polishing cloth using a 1 µm diamond suspension and a 0.05 µm alumina slurry. The scan rate was 50 $mV.s^{-1}$. Solutions of dry acetonitrile containing 0.1 M tetrabutylammonium perchlorate (TBAP) as the supporting electrolyte were bulk deaerated with Ar for at least 15 min before CVs. Bulk electrolysis experiments were carried out at room temperature in a custom-built, gas-tight two-compartment electrochemical cell specific for mercury that has been previously described.[25] The cathodic and anodic compartments are separated via a porous glass frit of fine porosity. . Bulk solutions, constantly stirred, of 0.5 mM of catalysts and 2 M of trifluoroethanol (TFEH) in acetonitrile containing 0.1 M TBAP were purged with CO_2 gas for 30 min before starting the experiment. The working electrode was a pool of 0.5 mL of mercury, the counter electrode was a 0.5 mm diameter platinum wire and the reference electrode was a saturated Ag/AgCl/KCl electrode. Carbon monoxide was detected with a gas chromatograph (Shimadzu GC-2010) equipped with a methanizer, a flame induction detector (FID), and a shincarbon ST (Restek) column. Formic acid concentrations were determined by

ionic exchange chromatography (883 Basic IC, Metrohm). H_2 was detected a gas chromatograph coupled to a thermal conductivity detector (Shimadzu GC-2014). Aliquots of gas were removed with a gas-tight syringe.

Computational Methods

All geometries were fully optimized at the B3P86[51,52]/6-311+G(d,p)[53,54] level of density functional theory (DFT) using the Gaussian 09 program[55] and the SMD implicit-solvation model,[56] for which acetonitrile (ε = 35.688) was chosen as the solvent, consistent with the experiment. Unrestricted Kohn-Sham formalism was used to explore the spin multiplicity of the investigated adducts. Harmonic vibrational frequencies were computed on the optimized geometries to ensure that all local minima display real frequencies only, whereas the transition states were characterized by a single imaginary frequency. The zero-point vibrational energies, thermal corrections and entropy terms for the optimized geometries were obtained from the frequency calculations. Reduction potentials were calculated using the equation $E^0 = \left(-\frac{\Delta G^0}{nF}\right) - E^0_{ref}$, where *n* is the number of transferring electrons, *F* is Faraday's constant, ΔG^0 is the free energy of reduction, corrected by 1.89 kcal mol^{-1} for the 1 atm to 1M standard-state concentration change, and E^0_{ref} is the absolute reduction potential of the reference species, (the ferrocenium/ferrocene couple (Fc^+/Fc)), computed at the same level of theory. The thus obtained reduction potentials were then converted to values *vs.* the Ag/AgCl electrode by adding 0.5 V. The free energy of reactions involving protons was calculated by explicitly considering the equilibria among TFEH and TFE^-/TFEH homoconjugate, and one or two TFEH molecules were used as an explicit proton source for the transition state barrier computations.

REFERENCES

1. Elgrishi, N.; Chambers, M. B.; Wang, X.; Fontecave, M. *Chem. Soc. Rev.* **2017**, *46*, 761-796.
2. Takeda, H.; Cometto, C.; Ishitani, O.; Robert, M. *ACS Catal.* **2017**, *7*, 70-88.
3. Elgrishi, N.; Chambers, M. B.; Fontecave, M. *Chem. Sci.* **2015**, *6*, 2522-2531.
4. Windle, C. D.; Perutz, R. N. *Coord. Chem. Rev.* **2012**, *256*, 2562-2570.
5. Appel, A. M.; Bercaw, J. E.; Bocarsly, A. B.; Dobbek, H.; DuBois, D. L.; Dupuis, M.; Ferry, J. G.; Fujita, E.; Hille, R.; Kenis, P. J.; Kerfeld, C. A.; Morris, R. H.; Peden, C. H.; Portis, A. R.; Ragsdale, S. W.; Rauchfuss, T. B.; Reek, J. N.; Seefeldt, L. C.; Thauer, R. K.; Waldrop, G. L. *Chem. Rev.* **2013**, *113*, 6621-6658.
6. Costentin, C.; Robert, M.; Saveant, J. M. *Acc. Chem. Res.* **2015**, *48*, 2996-3006.
7. Smieja, J. M.; Sampson, M. D.; Grice, K. A.; Benson, E. E.; Froehlich, J. D.; Kubiak, C. P. *Inorg. Chem.* **2013**, *52*, 2484-2491.
8. Beley, M.; Collin, J.-P.; Ruppert, R.; Sauvage, J.-P. *J. Chem. Soc., Chem. Commun.* **1984**, 1315-1316.
9. Beley, M.; Collin, J. P.; Ruppert, R.; Sauvage, J. P. *J. Am. Chem. Soc.* **1986**, *108*, 7461-7467.
10. Froehlich, J. D.; Kubiak, C. P. *Inorg. Chem.* **2012**, *51*, 3932-3934.
11. Froehlich, J. D.; Kubiak, C. P. *J. Am. Chem. Soc.* **2015**, *137*, 3565-3573.
12. Wu, Y.; Rudshteyn, B.; Zhanaidarova, A.; Froehlich, J. D.; Ding, W.; Kubiak, C. P.; Batista, V. S. *ACS Catal.* **2017**, *7*, 5282-5288.
13. Song, J.; Klein, E. L.; Neese, F.; Ye, S. *Inorg. Chem.* **2014**, *53*, 7500-7507.
14. Fisher, B.; Eisenberg, R. *J. Am. Chem. Soc.* **1980**, *102*, 7361-7363.
15. Kuehnel, M. F.; Orchard, K. L.; Dalle, K. E.; Reisner, E. *J. Am. Chem. Soc.* **2017**, *139*, 7217-7223.
16. Thoi, V. S.; Kornienko, N.; Margarit, C. G.; Yang, P.; Chang, C. J. *J. Am. Chem. Soc.* **2013**, *135*, 14413-14424.
17. Hong, D.; Tsukakoshi, Y.; Kotani, H.; Ishizuka, T.; Kojima, T. *J. Am. Chem. Soc.* **2017**, *139*, 6538-6541.
18. Jeoung, J.-H.; Dobbek, H. *Science* **2007**, *318*, 1461-1464.
19. Stein, B. W.; Kirk, M. L. *J. of Biol. Inorg. Chem.* **2015**, *20*, 183-194.
20. Dobbek, H. *Coord. Chem. Rev.* **2011**, *255*, 1104-1116.
21. Moura, J. J. G.; Brondino, C. D.; Trincao, J.; Romao, M. J. *J. Biol. Inorg. Chem.* **2004**, *9*, 791-799.
22. Das, A.; Han, Z.; Brennessel, W. W.; Holland, P. L.; Eisenberg, R. *ACS Catal.* **2015**, *5*, 1397-1406.
23. Zarkadoulas, A.; Field, M. J.; Papatriantafyllopoulou, C.; Fize, J.; Artero, V.; Mitsopoulou, C. A. *Inorg. Chem.* **2016**, *55*, 432-444.
24. Koshiba, K.; Yamauchi, K.; Sakai, K. *Angew. Chem. Int. Ed.* **2017**, *56*, 4247-4251.
25. Porcher, J. P.; Fogeron, T.; Gomez-Mingot, M.; Derat, E.; Chamoreau, L. M.; Li, Y.; Fontecave, M. *Angew. Chem. Int. Ed.* **2015**, *54*, 14090-14093.
26. Fogeron, T.; Porcher, J.-P.; Gomez-Mingot, M.; Todorova, T. K.; Chamoreau, L.-M.; Mellot-Draznieks, C.; Li, Y.; Fontecave, M. *Dalton Trans.* **2016**, *45*, 14754-14763.
27. Porcher, J. P.; Fogeron, T.; Gomez-Mingot, M.; Chamoreau, L. M.; Li, Y.; Fontecave, M. *Chem. Eur. J.* **2016**, *22*, 4447-4453.
28. Begum, A.; Moula, G.; Sarkar, S. *Chem. Eur. J.* **2010**, *16*, 12324-12327.
29. Fogeron, T.; Retailleau, P.; Chamoreau, L. M.; Fontecave, M.; Li, Y. *Dalton Trans.* **2017**, *46*, 4161-4164.
30. Chapovetsky, A.; Do, T. H.; Haiges, R.; Takase, M. K.; Marinescu, S. C. *J. Am. Chem. Soc.* **2016**, *138*, 5765-5768.
31. Costentin, C.; Drouet, S.; Robert, M.; Saveant, J. M. *Science* **2012**, *338*, 90-94.
32. Anderson, J. S.; Iluc, V. M.; Hillhouse, G. L. *Inorg. Chem.* **2010**, *49*, 10203-10207.
33. Beck, R.; Shoshani, M.; Krasinkiewicz, J.; Hatnean, J. A.; Johnson, S. A. *Dalton Trans.* **2013**, *42*, 1461-1475.

34. Dohring, A.; Jolly, P. W.; Kruger, C.; Romão, M. J. *Z. Naturforsch. B* **2014**, *40*, 484-488.
35. Aresta, M.; Nobile, C. F.; Albano, V. G.; Forni, E.; Manassero, M. *J. Chem. Soc., Chem. Commun.* **1975**, 636-637.
36. Sakaki, S.; Koga, N.; Morokuma, K. *Inorg. Chem.* **1990**, *29*, 3110-3116.
37. Dedieu, A.; Ingold, F. *Angew. Chem. Int. Ed. Engl.* **1989**, *28*, 1694-1695.
38. Sakaki, S. *J. Am. Chem. Soc.* **1992**, *114*, 2055-2062.
39. Keith, J. A.; Grice, K. A.; Kubiak, C. P.; Carter, E. A. *J. Am. Chem. Soc.* **2013**, *135*, 15823-15829.
40. Lam, Y. C.; Nielsen, R. J.; Gray, H. B.; Goddard, W. A. *ACS Catal.* **2015**, *5*, 2521-2528.
41. Schneider, J.; Jia, H. F.; Kobiro, K.; Cabelli, D. E.; Muckerman, J. T.; Fujita, E. *Energy Environ. Sci.* **2012**, *5*, 9502-9510.
42. Sawamoto, H. *J. Electroanal. Chem. Interfacial Electrochem.* **1980**, *113*, 301-304.
43. Ramirez, S.; Gordillo, G. J.; Posadas, D. *J. Electroanal. Chem.* **1996**, *407*, 219-225.
44. Farias, P. A. M.; Bastos, M. B. R. *Int. J. Electrochem.* **2013**, *2013*, 1-7.
45. Chen, L. J.; Guo, Z. G.; Wei, X. G.; Gallenkamp, C.; Bonin, J.; Anxolabehere-Mallart, E.; Lau, K. C.; Lau, T. C.; Robert, M. *J. Am. Chem. Soc.* **2015**, *137*, 10918-10921.
46. Taheri, A.; Thompson, E. J.; Fettinger, J. C.; Berben, L. A. *ACS Catal.* **2015**, *5*, 7140-7151.
47. Pun, S. N.; Chung, W. H.; Lam, K. M.; Guo, P.; Chan, P. H.; Wong, K. Y.; Che, C. M.; Chen, T. Y.; Peng, S. M. *J. Chem. Soc., Dalton Trans.* **2002**, 575-583.
48. Roy, S.; Sharma, B.; Peaut, J.; Simon, P.; Fontecave, M.; Tran, P. D.; Derat, E.; Artero, V. *J. Am. Chem. Soc.* **2017**, *139*, 3685-3696.
49. Collin, J. P.; Jouaiti, A.; Sauvage, J. P. *Inorg. Chem.* **1988**, *27*, 1986-1990.
50. Franco, F.; Cometto, C.; Vallana, F. F.; Sordello, F.; Priola, E.; Minero, C.; Nervi, C.; Gobetto, R. *Chem. Commun.* **2014**, *50*, 14670-14673.
51. Becke, A. D. *J. Chem. Phys.* **1993**, *98*, 5648-5652.
52. Perdew, J. P. *Phys. Rev. B* **1986**, *33*, 8822-8824.
53. McLean, A. D.; Chandler, G. S. *J. Chem. Phys.* **1980**, *72*, 5639-5648.
54. Krishnan, R.; Binkley, J. S.; Seeger, R.; Pople, J. A. *J. Chem. Phys.* **1980**, *72*, 650-654.
55. Frisch, M. J.; Trucks, G. W.; Cheeseman, J. R.; Scalmani, G.; Caricato, M.; Hratchian, H. P.; Li, X.; Barone, V.; Bloino, J.; Zheng, G.; Vreven, T.; Montgomery, J. A.; Petersson, G. A.; Scuseria, G. E.; Schlegel, H. B.; Nakatsuji, H.; Izmaylov, A. F.; Martin, R. L.; Sonnenberg, J. L.; Peralta, J. E.; Heyd, J. J.; Brothers, E.; Ogliaro, F.; Bearpark, M.; Robb, M. A.; Mennucci, B.; Kudin, K. N.; Staroverov, V. N.; Kobayashi, R.; Normand, J.; Rendell, A.; Gomperts, R.; Zakrzewski, V. G.; Hada, M.; Ehara, M.; Toyota, K.; Fukuda, R.; Hasegawa, J.; Ishida, M.; Nakajima, T.; Honda, Y.; Kitao, O.; Nakai, H. *Gaussian 09*, Gaussian Inc. Wallingford CT 2009.
56. Marenich, A. V.; Cramer, C. J.; Truhlar, D. G. *J. Phys. Chem. B* **2009**, *113*, 6378-6396.